Gain-swept superradiance applied to the stand-off detection of trace impurities in the atmosphere

V. Kocharovsky*, S. Cameron†, K. Lehmann‡, R. Lucht§, R. Miles¶, Y. Rostovtsev*, W. Warren‡, G. R. Welch*, and M. O. Scully*‡¶‖**

*Department of Physics and Institute for Quantum Studies and ‖Department of Electrical Engineering, Texas A&M University, College Station, TX 77843; †Sandia National Laboratory, Albuquerque, NM 87185; Departments of ‡Chemistry and ¶Mechanical and Aerospace Engineering, Princeton University, Princeton, NJ 08544; and §Department of Mechanical Engineering, Purdue University, West Lafayette, IN 47907

Contributed by M. O. Scully, April 7, 2005

We show that gain-swept superradiance can be used to detect low (parts per million) concentrations of various gases at distances on the order of kilometers, which is done by using pulse timing to create small regions of gain at positions that sweep toward a detector. The technique is far more sensitive than previous methods such as light detection and ranging or differential absorption light detection and ranging.

The continuous monitoring of the atmosphere for traces of various gases and biopathogens at parts-per-million (ppm) concentrations and distances of the order of 1–10 km is a challenging problem, with applications from the control of environmental pollution to national security [e.g., the monitoring of nitric oxide (NO) and the warfare gas phosgene ($COCl_2$)]. In the latter case, the LD_{50} (lethal dose for 50% for those exposed) is of the order of 10 ppm (1, 2). Continuous monitoring of the atmosphere for such gases at distances from 1 to 10 km would obviously be desirable and difficult. Beautiful measurements (3, 4) using light detection and ranging (LIDAR) techniques coupled with differential absorption LIDAR (DIAL) measurements have been reported and provide an important tool for the measurement of trace impurities in the atmosphere. However, to continuously scan the 2π sector of the sky covering a city, new schemes are needed. Stand-off superradiant (SOS) spectroscopy is such a scheme.

The detection scenario shown in Fig. 1 has two logical steps. In the first step, Raman or two-photon pumping of the gas molecules from the ground state to an appropriate excited state takes place. The excitation is achieved by simultaneous action of two synchronized picosecond laser pulses with a difference frequency that is resonant with the ground to vibrationally excited-state energy difference, or a sum frequency being resonant with the ground to electronically excited-state energy difference (5).

Then, in the second step, strong emission in the backward direction is generated by swept-gain superradiance (see refs. 6 and 7 and references therein). This generation ensures unidirectional high-gain propagation of the IR (Raman pumping) or UV (two-photon pumping) signal only within a narrow solid angle directed back along the exciting lasers, as shown in Fig. 1.

This scheme has the potential for real-time detection of poison gases (e.g., $COCl_2$) and atmospheric pollutants (e.g., NO). Clouds in the size range of 1 m to 1 km can be addressed at distances from 10 m to 100 km and beyond. The essential advantage of this scheme is that the signal intensity exceeds the backscattering signal intensity of the usual LIDAR schemes by many orders of magnitude.

SOS spectroscopy has the main useful features of standard LIDAR systems, e.g. (*i*) long-range remote sensing, (*ii*) ranging by recording the time delay of the "radar" pulse return signal, (*iii*) monostatic (one location) operation with only "one" instrument on a mobile platform, and (*iv*) simplicity of alignment and pointing. Furthermore, the present "superradiant LIDAR" combines these advantages with several other significant advances, e.g. (*i*) many orders of magnitude increase in the magnitude of the detected signal and sensitivity, (*ii*) the possibility of real-time spectrally selective sensing, and (*iii*) the measurement of density distributions.

Thus, the principle of the present SOS spectroscopy is completely different from the well known DIAL technique and has significant advantages. In the following analysis, the application to such simple gases as mentioned earlier is presented.

Analysis

Let us first consider a subpicosecond ground-based (or airborne) laser system that emits pairs of picosecond visible pulses as shown in Fig. 1. There is a time delay $\Delta t_{n,n+1}$ between the pulses in the nth pair. The first pulse in a pair is at a higher frequency (e.g., $\lambda_1 = 400$ nm), and the second pulse is at a lower frequency (e.g., $\lambda_2 = 580$ nm). The two pulses have different group velocities because of the dispersion of air. The delay time Δt_{12} between the first two pulses determines the distance z from the transmitter at which the faster-moving lower-frequency pulse catches up with the slower-moving higher-frequency pulse. Specifically, the group velocity in air depends on the frequency,

$$v_g(\omega) = \frac{\mathrm{d}\omega}{\mathrm{d}k} = (\mathrm{d}[\omega n(\omega)]/c\,\mathrm{d}\omega)^{-1} \approx c(1 + \lambda\,\mathrm{d}n/d\lambda). \quad [1]$$

Because of the dispersion of the refractive index of air (given by Cauchy's formula)

$$n(\lambda) = 1.000287566 + 1.34/\lambda^2(\mathrm{nm}) + 3.777 \times 10^4/\lambda^4(\mathrm{nm}), \quad [2]$$

the typical difference Δv_g between the group velocities of the two pulses is a few kilometers per second, that is $\Delta v_g = v_g(\omega_2) - v_g(\omega_1) \sim 4 \times 10^5$ cm/s for $\lambda_1 = 400$ nm and $\lambda_2 = 580$ nm.

Consider the nth pulse pair having an initial separation $\Delta L_n = c\Delta t_{n,n+1}$. They will overlap after a time τ_n (when the faster pulse overtakes the slower pulse) defined by $\Delta L_n = \Delta v_g \tau_n$. The pulses are each moving at essentially the speed of light in vacuum so that the distance (from the sender) at which the overlap occurs is given by $z_n = c\tau_n = c\Delta L_n/\Delta v_g$. Hence, if we want the nth pair to overlap in the vicinity of z_n, we should fix the separation to be $\Delta t_{n,n+1} = \Delta v_g z_n/c^2$. For the case of $\lambda_1 = 400$ nm and $\lambda_2 = 580$ nm discussed above, $\Delta t_{n,n+1} \approx 50$ ps for $z_n = 1$ km.

Choosing a time delay $\Delta t_{12} = z\Delta v_g/c^2$, we can ensure that two pulses in a pair overlap each other at a particular location z in the target cloud, e.g. at $z = 1$ km for $\Delta t_{12} \sim 50$ ps. Because each

Abbreviations: LIDAR, light detection and ranging; DIAL, differential absorption LIDAR; SOS, stand-off superradiant.

**To whom correspondence should be addressed. E-mail: scully@tamu.edu.

www.pnas.org/cgi/doi/10.1073/pnas.0500534102

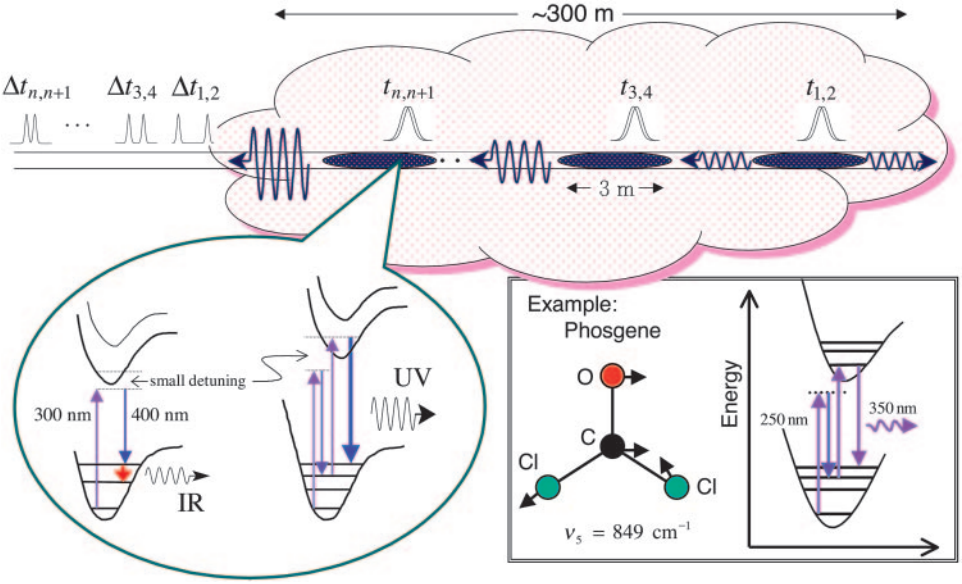

Fig. 1. SOS spectroscopy. Multiple pairs of pulses are generated such that the spacing between pulses in each pair is decreasing. The second pulse in each pair has a higher velocity because of atmospheric dispersion. The first pair of pulses overlaps near the back of the cloud, creating a small region of gain. Subsequent pairs overlap at closer and closer regions of the cloud, producing a swept-gain amplifier that lases back toward the observer. We suggest two schemes: one in which blue and UV pulses are sent toward the cloud, causing lasing on an IR vibrational transition, and the other in which IR and UV pulses are sent toward the cloud, causing lasing on a blue electronic transition (such as the example shown in phosgene).

pulse has a temporal duration of ~1 ps, the spatial length of a pulse is of the order of $\Delta L_{\text{pulse}} \sim c \times 1$ ps $\sim 3 \times 10^{-2}$ cm, where $c = 3 \times 10^{10}$ cm/s is the velocity of light in vacuum. Hence, the two pulses are overlapping along the propagation path for a length of the order of $\Delta L_{\text{overlap}} = \Delta L_{\text{pulse}} c/\Delta v_g \sim 20$ m. Over a portion, ΔL_{pump}, of this overlap length the two pulses with properly chosen amplitudes will produce the desired stimulated Raman adiabatic passage (STIRAP) pumping of the vibrational transition or two-photon pumping of the UV electronic transition. (In particular, pump amplitudes are chosen so that their Rabi frequencies times the pulse duration is greater than π.) In such a case, counterintuitive passage (STIRAP) can be used. Under such conditions, a robust (≈100%) population inversion on the vibrational transition $v = 4 \rightarrow v = 3$ or UV electronic transition as shown in Fig. 1 is possible. Note that ΔL_{pump} is estimated as

$$\Delta L_{\text{pump}} \sim 0.1 \Delta L_{\text{overlap}} = 0.1 \Delta L_{\text{pulse}} c/\Delta v_g \sim 2 \text{ m}. \quad [3]$$

The relaxation time of the population inversion caused by collisions in the air is in the nanosecond range, $T_1 \sim 1$ ns. Therefore, as indicated in Fig. 1, each pair of visible pump pulses should follow the previous pair by the time T_{rep} of order $T_1 \sim 1$ ns. In addition, we repeatedly decrease the delay time $\Delta t_{n,n+1}$ between pulses in successive pairs by an amount $T_{rep}\Delta v_g/c \sim 0.01$ ps. Because of this sequential decrease of the delay time between the two members of a given pulse pair $\Delta t_{n,n+1}$, the gas along the LIDAR return path is pumped in neighboring segments that are successively closer to the receiver by approximately $cT_{rep} \sim 0.3$ m. With such a sequence of pairs of visible pump pulses (having $\Delta t_{n,n+1}$ properly decreased in successive pairs), a long swept-gain amplifier of IR vibrational or UV electronic transition radiation in the warfare-gas cloud being interrogated is created. This amplifying region of excited gas molecules is a narrow cylinder of cross-sectional area A_s determined by the optics as illustrated in Fig. 2. This swept-gain configuration yields a beam of exponentially amplified spontaneous IR or UV radiation that is gain-guided in the backward direction. Note that the radiation from a particular vibrational transition, e.g., $v = 4 \rightarrow v = 3$, is not reabsorbed by molecules in other vibrational states (e.g., $v = 0 \rightarrow v = 1$) because of the anharmonicity of the molecular oscillator.

Also, because the wavelength of the mid-IR radiation is of the order $\lambda \sim 10$ μm, the radiation propagates with very little absorption because of the well known atmospheric transparency windows in the wavelength range from 3 to 5 μm and from 7 to 12 μm. Likewise, in the case of UV emission, the offset of the ground and electronic states allows for population inversion. Atmospheric propagation is possible without absorption in many applicable wavelength regions.

The regime of amplification in the long swept-gain amplifier described above depends on, among other things, the density of the pumped gas molecules N and the length L of the pumped region in the cloud. As discussed in refs. 6 and 7, the standard gain g is given by

$$g = \alpha' T_2 = 4\pi\wp^2\omega_0 \Delta N T_2/c\hbar = 3(\lambda_{\text{IR}}^2/4\pi)\gamma_0 \Delta N T_2, \quad [4]$$

where T_2 is the phase relaxation time ($T_2 < T_1 \sim 1$ ns), γ_0 is the radiative rate of decay from the upper to the lower operating state, ΔN is the density of the population difference of the warfare-gas molecules at the operating transition, $\omega_0 = 2\pi c/\lambda_0$ and $\wp$ are the frequency and dipole moment of this transition, respectively, and $\omega_c = 2\sqrt{\alpha' c} = 2/T_c$ is the cooperative frequency (as defined and discussed in ref. 6) that determines the rate of correlation of molecules through their interaction via exchange of emitted photons.

Next, consider the population, ΔN, in the upper of the two levels, e.g., $v = 4$ in the IR case. At $\lambda = 10$ μm we may take the populations in the state $v = 3$ to be essentially zero. To easily transfer a substantial population from the $v = 0$ level into, say, the $v = 4$ level or the electronic excited state, we prefer to operate in single-photon resonance. As indicated in Fig. 1, the resonant Raman case involves replacing the visible radiation by UV. The associated resonant UV scheme of Fig. 1 operates by absorption of IR ($v = 0$ to $v = 1$) and UV (electronic ground to excited state), which occurs when the IR and UV pump pulses overlap. By tailoring the drive pulses properly, we can arrange to

PHYSICS

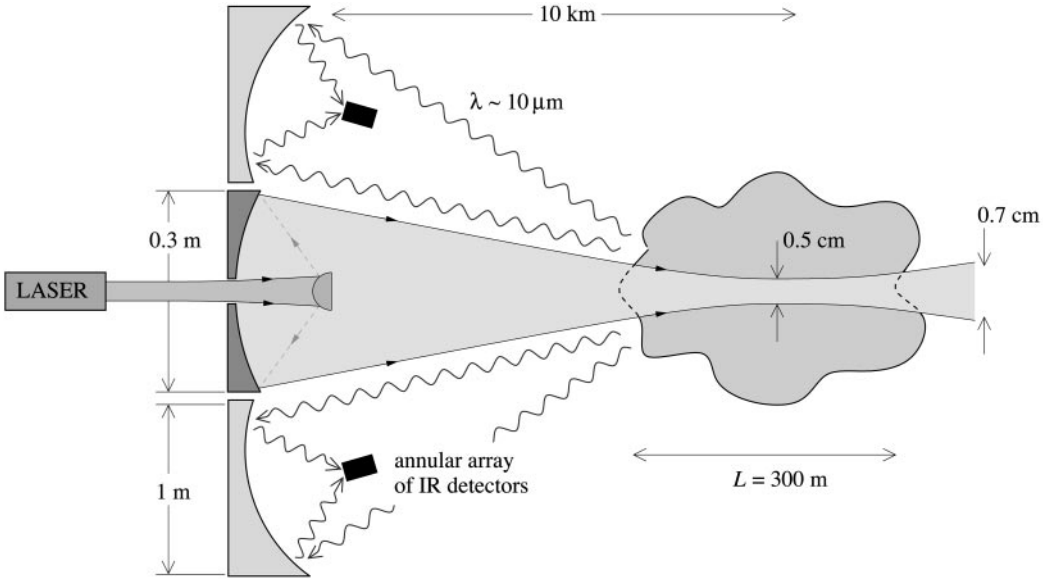

Fig. 2. Schematic of the experimental apparatus.

have a very substantial fraction of the $v = 0$ molecules brought into the excited state. This happens when $\wp E_{\text{drive}}\tau/\hbar \gtrsim \pi$, where τ is the pulse duration $\approx 10^{-12}$ s. Thus, we require $E_{\text{drive}} \gtrsim \pi\hbar/\wp\tau$, implying an energy per pulse of

$$W \gtrsim \varepsilon_0 E_{\text{drive}}^2 A c \tau \approx \varepsilon_0 [\pi^2\hbar^2/\wp^2\tau] A c.$$

For example, if $\wp = ea_0 \approx 10^{-29}$ Coulomb meter, the energy in each picosecond pulse is only a fraction of a millijoule.

Amplification Process

The evolution of the amplification process (see Fig. 3) of the backward mid-IR or UV signal is characterized by the following four different regimes.

Linear Amplification of Vacuum Fluctuations (or Thermal Radiation). In this regime the total gain along the whole gain-swept amplifier of a length L is small, $(g - \kappa)\, L \ll \ln \phi_0^{-1}$, where κ is the linear radiation losses in the amplifier caused by absorption, scattering, and diffraction out of the pumped cylindrical active region. The latter diffraction losses are determined by the cross-sectional area A_s as $\kappa_{\text{diff}} \sim \lambda_0/(3A_s)$. The variance of the Bloch angle at the operating transition characterizes the spontaneous or thermal noise, $\phi_0 \sim (NA_s\, L)^{-1/2} \ll 1$, and is small, typically $\ln \phi_0^{-1} \sim 30$. The spatial profile of the average intensity of this amplified spontaneous (or thermal) luminescence along the gain-swept path in the cloud is a simple exponent,

$$I = I_{\text{noise}} \exp(2(g - \kappa)z), \qquad [5]$$

and there is no any significant saturation of the population difference ΔN. In other words, the signal intensity, emitted from the cloud, is less than the saturation value: $I(z = L) < I_{\text{sat}} = c\hbar^2/8\pi\wp^2 T_1 T_2$. The pulse duration of the luminescence signal is of the order of $\tau \sim \tau_L = T_1$.

Pulsed Superluminescence (Nonlinear Gain in Rate Equation Approximation). In this regime the gain is relatively large, $\ln \phi_0^{-1} \lesssim (g - \kappa)\, L \ll (\ln \phi_0^{-1})^2/4$. The last inequality implies, however, that the cooperative time $T_c = (\alpha' c)^{-1/2}$ is still longer by a factor of $(\ln \phi_0^{-1})/2$ than the phase relaxation time on the operating transition, $T_c \gg 2T_2/\ln \phi_0^{-1}$. The superluminescent-pulse duration again is determined by the relaxation time of the population inversion in the gain-swept amplifier, $\tau \sim \tau_{\text{SL}} \sim T_1$. The intensity of the superluminescent pulse at the exit from the cloud is much larger than that of the spontaneous luminescence and is proportional to the number of pumped molecules,

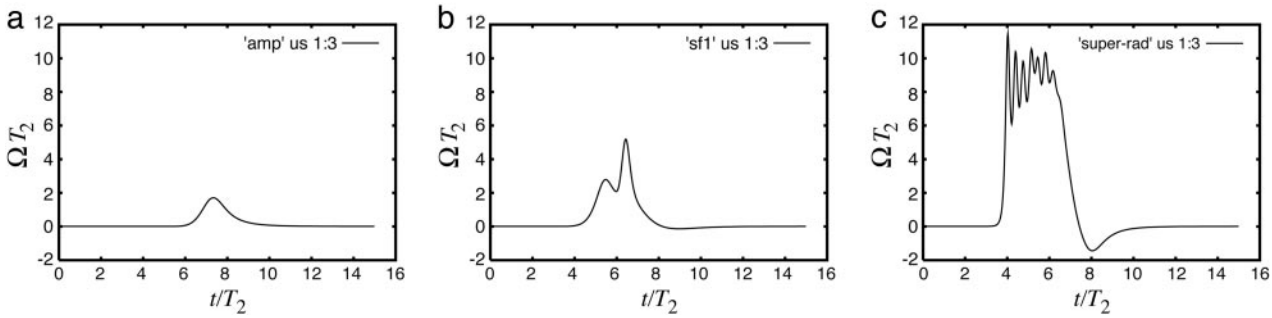

Fig. 3. Snapshots of the generated pulse at different positions in the cloud: at the far edge of the cloud where the pulse experiences linear amplification (*a*); in the middle of the cloud where the superfluorescent pulse is formed (*b*); and at the near edge of the cloud where the superradiant pulse is formed, where one can see that the time scale of the ringing is smaller than T_2 (*c*). Parameters used in the simulation are: $\wp = 0.1D$, $N = 10^{14}$ cm^{-3}, and $T_2 = 10^{-9}$ s. Our estimate is that by using 60 laser pulses to transfer population to the excited vibrational state to create population inversion, one photon of spontaneous radiation at the far edge of the cloud will be amplified to 10^{16} photons leaving the near edge.

$$I_{SL} \sim 0.5c\hbar\omega_0 NL\tau_{SL}^{-1} \exp(-2\kappa L). \quad [6]$$

The latter corresponds to the pulse energy that is of the order of half of the total pump energy stored at the operating transition in the warfare-gas molecules,

$$W \sim W_{SL} = I_{SL}A_s\tau_{SL} = 0.5\hbar\omega_0 NLA_s, \quad [7]$$

if one would ignore losses. The spatial-temporal behavior of the superluminescent pulse traveling through the gain-swept amplifier can be described on the basis of the rate equations and is well studied (see, e.g., refs. 6–8 and references therein). It can be qualitatively inferred from the following simple equation for the field intensity of the signal

$$\frac{\partial I(t,z)}{\partial z} = -2\kappa I + 2gI/(1 + I/I_{sat}), \quad [8]$$

which is valid in the case of relatively long pulses ($\tau \gg T_1$) when the population difference is adiabatically saturated by the instantaneous value of the intensity, $\Delta N = N/(1 + I/I_{sat})$.

Superradiance (Superfluorescence). This coherent regime of the cooperative spontaneous (or thermal) emission occurs when the gain is very large, $gL \gtrsim (\ln \phi_0^{-1})/4$ so that the delay time of the development of superradiance (which in long-enough amplifiers is of the order of $t_D \sim T_c \ln \phi_0^{-1}$) is shorter than the population relaxation time, $T_D < T_1$. The superradiant regime provides a possibility to shorten the pulse duration below the relaxation time scale T_2 and to increase further the maximal signal intensity. The linear-stage growth of the intensity of the superfluorescence from the noise level with the time t after pumping explicitly depends on the amplification length z, namely

$$I_{SR} \sim I_{noise} \exp\left[2\left(4\alpha'\left(t - \frac{z}{c}\right)z\right)^{1/2}\right]. \quad [9]$$

The latter result and, in particular, the characteristic space-time profile of the superradiant pulse as a function of the combined variable $\sqrt{(t - z/c)z}$ can be derived from the fact that one-dimensional Maxwell–Bloch equations for the complex slow-varying amplitudes of the field E and polarization P of the plane wave $\propto exp(-i\omega_0 t + i\omega_0 z/c)$ in the RWA approximation, namely

$$\frac{1}{c}\frac{\partial E}{\partial t} + \frac{\partial E}{\partial z} + \kappa E = 2\pi i\frac{\omega_0}{c}P, \quad [10]$$

$$\frac{\partial P}{\partial t} + \frac{P}{T_2} = \frac{-i\omega_c^2}{8\pi\omega_0}E, \quad [11]$$

$$\frac{\partial \Delta N}{\partial t} + \frac{\Delta N - \Delta N_0}{T_1} = \frac{1}{\hbar}Im(E^*P), \quad [12]$$

have the modified Bessel functions $I_0(\zeta')$ and $I_1(\zeta')$ of the variable

$$\zeta' = \frac{\omega_c}{c}[(z - z')(ct - (z - z'))]^{1/2} \quad [13]$$

as the main part of their Green function at the linear stage of evolution, when $\Delta N = N =$ constant. Indeed, for the arbitrary initial profiles of the polarization $P(z, t = 0) = P_0(z)\Theta(z)$ and field $E(z, t = 0) = E_0(z)\Theta(z)$ and arbitrary incident field $E(z = 0, t) = E_{in}(t)\Theta(t)$, we have from Eqs. **10** and **11** the following general solution (7) in the case of fixed population inversion $\Delta N = N =$ constant:

$$E(z,t) = \theta(\tilde{t})e^{-\kappa z}\left\{E_{in}(\tilde{t}) + \int_0^{\tilde{t}} E_{in}(t')e^{-(\tilde{t}-t')/T_2}\frac{\omega_c}{2}\cdot\left(\frac{z/c}{\tilde{t}-t'}\right)^{1/2} I_1\left(\frac{\omega_c}{c}[c(\tilde{t}-t')z]^{1/2}\right)dt'\right\}$$
$$+ \frac{2\pi i\omega_0}{c}e^{-t/T_2}\int_0^z P_0(z')\exp\left[(z-z')\left(\frac{1}{cT_2} - \kappa\right)\right]\cdot\theta\left(\tilde{t} - \frac{z'}{c}\right)I_0(\zeta')dz' + E_0(z - ct)e^{-\kappa ct}$$
$$+ \frac{1}{2}e^{-t/T_2}\int_0^z\left\{E_0(z')\exp\left[(z-z')\left(\frac{1}{cT_2} - \kappa\right)\right]\cdot\theta\left(\tilde{t} - \frac{z'}{c}\right)\zeta' I_1(\zeta')(c\tilde{t} - z')^{-1}\right\}dz'. \quad [14]$$

Here Θ is the Heaviside step function and $\tilde{t} = t - z/c$. It is straightforward to see from Eq. **14** that after a long-enough time the field and polarization on the linear stage of superradiance follow the similar asymptotic laws at all points of the active region, and these laws do not depend on the initial (smooth) profiles but only on the boundary value of the initial polarization $P_0(z = 0)$, namely

$$P(z,t) = \frac{c\zeta E(z,t)}{4\pi i\omega_0 z} = \frac{P_0(0)}{\sqrt{2\pi\zeta}}\exp(\zeta - \kappa z - t/T_2). \quad [15]$$

The spatial-temporal dynamics of the amplitude of the molecular polarization $P = -i\wp N \sin\phi$, the population inversion $\Delta N = N\cos\phi$, and the amplitude of electric field $E = (\hbar/\wp)\,\partial\phi/\partial t$ at the nonlinear stage of superradiance may be deduced from the one-dimensional sin-Gordon equation (equation 2.2 from ref. 6) that follows from Eqs. **10–12**:

$$\frac{\partial^2\phi}{\partial z\partial(t - z/c)} + \kappa\frac{\partial\phi}{\partial(t - z/c)} = \alpha'_N \sin\phi, \quad [16]$$

$$\alpha'_N = \alpha' N/\Delta N. \quad [17]$$

In the case of negligibly small linear losses, it can be described by a one-parameter family of its nonsingular self-similar solutions that obey the simple ordinary differential equation

$$\frac{d^2\phi}{d\zeta^2} + \zeta^{-1}\frac{d\phi}{d\zeta} = \sin\phi, \quad \zeta = 2(\alpha'_N(t - z/c)z)^{1/2}. \quad [18]$$

The superradiant pulse duration and delay time of its formation caused by the process of mutual correlations of warfare-gas molecules through the exchange by photons are inversely proportional to the square root of the warfare-gas density,

$$\tau_{SR} \sim 2T_c \propto N^{-1/2}, \quad [19]$$

$$t_{SRdelay} \sim \zeta_0\tau_{SR} \sim 30\tau_{SF}, \quad [20]$$

where $\zeta_0 \sim \ln\sqrt{I_{max}/I_{noise}} \sim \ln\phi_0^{-1} \sim 30$. The most important feature of the superradiance is that the warfare-gas molecules tend to emit photons cooperatively as a collective, macroscopic coherent dipole in each causally related subvolume

$V_c = A_s L_c \ln \phi_0^{-1}$ of the cooperative length $L_c \ln \phi_0^{-1} = cT_c \ln \phi_0^{-1}$ within the time durations shorter than the phase relaxation time, $\tau_{SR} < T_2$.

If one increases the gain further and pumps simultaneously very long active region, $L \gg L_c \ln \phi_0^{-1}$, then each causally related subvolume V_c would emit its own superradiant pulse with the duration τ_{SR} so that the whole active region would emit a chaotic sequence of many ($L/L_c \ln \phi_0^{-1} \gg 1$) such pulses with no additional increase of the peak intensity. However, we can overcome this unfavorable scenario by implementation of the gain-swept superradiance, as described below.

π-Pulse Production in a Long Swept-Gain Superradiant Amplifier. This gain-swept superradiant regime occurs when the gain is very large, $gL \gg (\ln \phi_0^{-1})^2/4$, and a coherent pulse is formed just behind the running front of pump pulses when the amplification length z is much larger than the cooperative length, $z \gg L_c \ln \phi_0^{-1}$. In this case, the swept-gain amplifier produces a time-dependent pulse (7) of duration $\tau_\pi \propto 1/z$, which is shorter than τ_{SR} (see Eq. **19**). The field amplitude of the pulse grows linearly with the length of amplification, $E \propto z$, and the pulse area tends to π,

$$\int \wp E(z, t)\mathrm{d}t/\hbar \approx \pi. \qquad [21]$$

This π-pulse takes up the entire energy stored in the pumped medium. Its asymptotic behavior is quasi-self-similar with the amplitude

$$E(z, t) = \frac{\hbar c z}{2\wp \zeta L_c^2} \frac{\partial \phi}{\partial \zeta}. \qquad [22]$$

This solution is determined by the function $\phi(\zeta)$ given by Eq. **18**, in which for each value of the self-similar variable ζ there are two coordinates,

$$z_{1,2} = \{ct \pm [(ct)^2 - 4\zeta^2 L_c^2]^{1/2}\}/2, \qquad [23]$$

that are related to two propagating fronts of population depletion. The population inversion ΔN first vanishes for $\zeta = \zeta_0 \sim \ln \phi_0^{-1} \gg 1$, i.e., in a time $t_0 = 2\zeta_0 L_c$ at the point $z_0 = \zeta_0 L_c$, where $z_1 = z_2$. For $t \to \infty$, one depletion front $z_1^{(0)} = z_1(\zeta = \zeta_0)$ approaches the beginning of the amplifier, $z_1^{(0)} \approx \zeta_0^2 L_c^2/ct \to 0$; the second depletion front $z_2^{(0)} = z_2(\zeta = \zeta_0)$ follows the pumping front, $z_2^{(0)} \approx ct$. The former generates the self-similar superradiant pulse in a short sample, $L \leq L_c \ln \phi_0^{-1}$, and the latter produces a time-dependent π-pulse in the long gain-swept superradiant amplifier.

The growth of this pulse is limited by radiation losses κ. If the gain is large enough, namely $g \gg \kappa \ln \phi_0^{-1}$, it results in the formation of a steady-state hyperbolic-secant superradiant pulse at large enough amplification length $L \gtrsim \ln \phi_0^{-1}/4\kappa$. This pulse has a sech-shaped profile

$$E_s = \frac{\hbar}{\wp \tau_s} \mathrm{sech}\left(\frac{t - z/c}{\tau_s}\right). \qquad [24]$$

Its time duration is shorter than T_2 and inversely proportional to the density of molecules

$$\tau_s = T_2 \kappa/g = c\hbar\kappa/4\pi\wp^2\omega_0 N_0, \qquad [25]$$

as in equations 1.7 and 1.9 in ref. 6. The intensity grows as the square of the density of initially excited molecules $N_0 = \Delta N$ ($t = 0$), i.e., $I_s \propto N_0^2$.

If one compares these results against the case of uniform excitation, one sees that here there is no limitation on the power, whereas in the other case, the pulse width can be no shorter than the cooperation time $T_c = (\alpha' c)^{-1/2}$, and thus the peak power is also limited. In uniform excitation there is a limitation on a maximal range of cooperation $L \ll L_c \ln \phi_0^{-1}$, which comes from the requirement that the atom must still be excited and avoid emission of photon until the pulse arrives. In a swept-gain amplifier, because atoms are excited only when the light coming from the proceeding ones reaches them, it is not necessary to impose a causal-related limit on the sample, i.e., the equivalent length of possible cooperation can be much larger than $L_c \ln \phi_0^{-1}$.

Estimates

Which amplification regime is realized depends first of all on the density N and size L of the warfare-gas cloud. For example, consider a typical vibrational transition with $\lambda_0 \sim 10$ μm, $\omega_0 \sim 2 \times 10^{14}$ s^{-1}, $\wp \sim 0.1$ D, and $T_{1,2} \sim 1$ ns. The values of the cooperative time and gain are then given by Eq. **4**, where we assume $\Delta N \sim N$,

$$T_c(s) \sim 10^{-2} N^{-1/2}(\mathrm{cm}^{-3}), \qquad [26]$$

$$g(\mathrm{cm}^{-1}) \sim 0.5 \times 10^{-15} N(\mathrm{cm}^{-3}). \qquad [27]$$

Consider an extremely low density of the warfare gas, $N \leq 2 \times 10^{14}$ cm^{-3} that is <10 ppm. Then, without a swept scheme, one has either amplified spontaneous emission [as discussed in *Linear Amplification of Vacuum Fluctuations (or Thermal Radiation)*] if the cloud size is small enough, L (cm) $< 10^{17}/N$ (cm^{-3}) or pulsed superluminescence [as discussed in *Pulsed Superluminescence (Nonlinear Gain in Rate Equation Approximation)*] if L (cm) $> 10^{17}$/N (cm^{-3}). In this case, the gain can be already very large, e.g. $e^{2gL} \sim e^{20} \approx 10^9$ for a cloud length $L \sim 10$ m and a density $N \sim 2 \times 10^{13}$ cm^{-3}, i.e. 1 ppm.

Consider larger densities, $N > 2 \times 10^{14}$ cm^{-3}, which still correspond to a very small fraction of the warfare gas in the air, only >10 ppm. Then the superradiance or π-pulse gain-swept coherent regime occurs with a huge gain $gL \gg 1$ and extreme pulse shortening. For example, at a marginal density $N \sim 2 \times 10^{14}$ cm^{-3} the superradiant pulse duration, τ_{SR} (s) $\sim 2 \times 10^{-2} N^{-1/2}$ (cm^{-3}), and the cooperative length, L_c (cm) $\sim 3 \times 10^8 N^{-1/2}$ (cm^{-3}), are $\tau_{SR} \sim 1$ ns and $L_c \sim 10$ cm, respectively, so that $L_c \ln \phi_0^{-1} \sim 3$ m; at a density $N \sim 10^{15}$ cm^{-3}, these become $\tau_{SR} \sim 0.5$ ns and $L_c \sim 5$ cm, respectively. The peak coherent mid-IR power emitted toward the receiver by the superradiant pulse from even each subvolume of cooperative length, $V_c = A_s L_c \ln \phi_0^{-1}$, is very large: for a density $N \sim 2 \times 10^{14}$ cm^{-3}, it is $I_{SR} \sim 4\hbar\omega_0 V_c N/\tau_{SR} A_s \ln \phi_0^{-1} \sim 10^6$ W/cm^2. This gain-collimated return signal propagates toward the receiver within the diffraction solid angle $\Delta\Omega \sim \lambda_0/L_c \ln \phi_0^{-1} \sim 10$ μm/3 m $\sim 3 \times 10^{-6}$ and can be detected easily from distances of many kilometers.

In the regime of the π-pulse in the gain-swept superradiance, the intensity at the exit from the cloud is even larger by a factor depending on $L/L_c \ln \phi_0^{-1}$. In a long-enough amplifier, when the steady-state π-pulse regime is formed, the intensity from the cloud reaches a peak value,

$$I_s = \frac{c}{8\pi} E_s^2 = \frac{c\hbar^2}{8\pi\wp^2\tau_s^2} \propto N_0^2, \qquad [28]$$

that is $I_s \sim 40$ MW/cm^2 with a pulse duration $\tau_s = T_2\kappa/g \sim 20$ ps for a density $N \sim 2 \times 10^{14}$ cm^{-3} and diffraction losses $\kappa = \lambda_0/3A_s \sim (500 \text{ cm})^{-1}$ in an amplifier of a diameter 0.5 cm (as shown in Fig. 2). In this case, the intensity at the receiver at a distance of 10 km from a cloud is of the order of 4 W/cm^2, because the diffraction solid angle is $\Delta\Omega \sim \lambda_0^2/A_s \sim 4 \times 10^{-6}$.

For example, the simulations shown in Fig. 3 predict the returning IR intensity at the near edge of the cloud to be of the order 10^6 W/cm^2, with a pulse energy of 6 mJ (so that the number of photons returning is 3×10^{16}).

To estimate the background noise from solar radiation scattered by haze, we assume horizontal observation and ~30% of scattering from regular clouds, or $\sim 5 \times 10^{-3}$ W·cm^{-2}·steradian^{-1} in the visible region of spectrum (neglecting the Fraunhofer dark bands). This corresponds to $\sim 10^{16}$ photons per s per steradian per cm^2 of observed scattering cross-sectional area. At 1 km, the solid angle for a 1-m diameter aperture is 10^{-6} steradian (although the presence of haze makes this rather uncertain). If we assume that the haze is colocated with the gas cloud, then the detector only observes that area that is illuminated by the laser, or ~1 cm^2, giving an unfiltered background of 10^{10} photons per s. Spectral filtering reduces this by $\sim 10^{-6}$ per GHz of bandwidth. The Raman signal may be broadened to several wavenumbers by rotational transitions; thus, we take the filter to be ~100 GHz, reducing the background to 10^6 photons per s. Finally, we can use time gating to further reduce the background. For a 300-m cloud, the light travel time is 1 μs, resulting in a filtered and time-gated solar background of 1 photon per laser shot. (Note that the distance to the cloud is not a factor in the time gating.)

These estimates are better in the blue because of the reduced solar flux but worse because of the wavelength dependence of Rayleigh scattering and haze; however, this estimate suggests that the solar background from haze at 1 km cannot be removed to levels <1 photon per 1 μs time window. One of the advantages of stimulated Raman and IR is that gain narrowing collapses the spectrum, so a narrower spectral filter might be used.

Discussion

For comparison with the technique of SOS spectroscopy introduced in this article, we briefly review here state-of-the-art techniques for detection of atmospheric ozone by DIAL (3) and atmospheric water-vapor concentration by Raman LIDAR (4).

The DIAL system developed by Walther and coworkers (3) for measurements of atmospheric ozone was based on the use of an injection-locked XeCl laser operating at 308 nm with a pulse energy of 150 mJ, a repetition rate of 50 Hz, and a line width of ~1 cm^{-1}. The 308-nm fundamental output of the XeCl laser is in the wing of a strong absorption band for ozone. A Raman-shifted Stokes beam at either 338 or 353 nm was generated in a Raman cell containing either methane or hydrogen, respectively. This Raman-shifted Stokes beam was not absorbed by ozone. Both the fundamental and Raman-shifted beams from the XeCl laser were expanded, collimated, and directed into the atmospheric region of interest. Backscattering from each beam caused by Rayleigh scattering was collected by using a 60-cm-diameter mirror, and the Rayleigh signals were measured by using a two-channel detection system with interference filters and three-stage Fabry–Perot filters for each wavelength. The ozone concentration was determined from the relative changes in the backscattered Rayleigh signals for the absorbed beam at 308 nm and the nonabsorbed beam at 338 or 353 nm. The quoted sensitivity of the system is 80 μg/m^3, corresponding to 0.04 ppm, for a 5-hour measurement time.

Bisson *et al.* (4) describe a Raman LIDAR system based also on an injection-locked XeCl laser system. Their Raman LIDAR instrument was developed for both daytime and nighttime measurements of atmospheric water vapor. For the Raman measurements, detection channels for Rayleigh scattering at 308 nm, N_2 Raman scattering at 331 nm, and H_2O Raman scattering at 347 nm were used. For the daytime measurements, it was critical to reduce the number of background photons to the absolute minimum level, and the system incorporated specialized optics to restrict the field of view and specialized interference filters to block UV photons outside the Raman detection channel. The system was capable of water-vapor concentration measurements at altitudes up to 5 km with a spatial resolution of 75 m and a temporal resolution of 5 min. However, the sensitivity is not sufficient for the present purposes.

In conclusion, the SOS scheme is capable of detecting trace impurities at the parts-per-million level at kilometer distances.

1. Ellison, D. H. (2000) *Handbook of Chemical and Biological Warfare Agents* (CRC, Boca Raton, FL).
2. Clayton, G. D. & Clayton, F. E. (1982) *Patty's Industrial Hygiene and Toxicology* (Wiley, New York), Vol. 2C.
3. Steinbrecht, W., Rothe, K. W. & Walther, H. (1989) *Appl. Opt.* **28,** 3616–3624.
4. Bisson, S. E., Goldsmith, J. E. M. & Mitchell, M. G. (1999) *Appl. Opt.* **38,** 1841–1849.
5. DePristo, A., Rabitz, H. & Miles, R. (1980) *J. Chem. Phys.* **73,** 4798–4806.
6. Bonifacio, R., Hopf, F. A., Meystre, P. & Scully, M. O. (1975) *Phys. Rev. A* **12,** 2568–2573.
7. Zheleznyakov, V. V., Kocharovsky, V. V. & Kocharovsky, Vl. V. (1989) *Sov. Phys. Usp.* **32,** 835–870.
8. Sargent, M., III, Scully, M. O. & Lamb, W. E. (1974) *Laser Physics* (Addison–Wesley, Reading, MA).